RESEARCH ARTICLE OPEN ACCESS

Automatic Segmentation of Ring Enhancing Lesions from T1 C+ and FLAIR MRI Images

R. Anita Jasmine, Dr.P. Arockia Jansi Rani
Department of Computer Science and Engineering
Manonmaniam Sundaranar University, Tirunelveli,
Tamil Nadu - India

ABSTRACT
The differential diagnosis of Ring Enhancing Lesion (REL) is done by analysing the different pattern on ring enhancement, surrounding vasogenic edema presence and nature of ring mass. In this paper, a quantitative analysis is done for texture and shape feature descriptors for automatically segmented REL images. A new efficient method for automatic REL segmentation from T1 C+ and FALIR MRI images is performed in two phases based on histogram thresholding and region growing techniques. Statistical, Tamura, Fourier coefficients, Invariant moment's descriptors are used to extract features and analysed using Wilcoxon Matched pairs rank sum Test.

Keywords: —T1C+, FLAIR, MRI, REL, Segmentation, feature analysis

I. INTRODUCTION

A Ring Enhancing Lesion (REL) is an abnormal radiologic sign obtained using radiocontrast medium which improves the visualization of anatomical internal structure. REL are characterized by an area of decreased density surrounded by a bright rim from concentration of the enhancing dye. Contrast enhanced Magnetic Resonance Imaging(MRI) or CT images are used to diagnose REL. Magnetic Resonance Imaging(MRI) is a non ionizing technique based on the phenomenon of nuclear magnetic resonance(NMR) that uses radio frequency(200 MHz – 2GHz) electromagnetic radiation and large magnetic fields around 1-2 tesla.

MRI images provide anatomical and physiological details in structure and function with 3D orientation, excellent soft tissues visualization and high spatial resolution [1]. FLAIR sequences are evaluated in diseases of central nervous system. In T1 C+ image the ring enhancement pattern is hyper intense and FLAIR image is hyper intense with peritumoural edema. Radiological analysis of REL is based on the intensity of ring, circularity of ring, no of rings and completeness of ring.

In this paper a new technique for automatic segmentation of ring enhancing lesions from T1 C+ and FLAIR images is proposed based on histogram thresholding and region growing approaches.Shape descriptors are used to differentiate the ring shape and texture descriptors are used to characterize the nature of ring mass and analysed. The rest of the paper is organized as follows: section 2 presents the literature survey from conventional to recent methods for segmentation, section 3 describes the proposed method for segmentation, section 4 details the feature descriptors used for texture and shape feature extraction, section 5&6 analyses the results of segmentation and features qualitatively and quantitatively. Section 7 ends up with conclusion, limitations and future work.

II. LITERATURE SURVEY

Several techniques are proposed to overcome the challenges in brain tumor detection and segmentation. Based on the degree of human interaction, brain tumor segmentation can be manual, semi automatic or fully automatic [2]. Manual segmentation needs brain anatomy knowledge to select the boundaries of segmentation and so error prone. Semi automatic methods need user interaction to initialize certain parameters. It involves initialization, feedback response and evaluation [3].The evaluations will be different from different persons and result in confusion. Fully Automatic segmentation methods are based on artificial intelligent techniques and prior knowledge. But they [4] do not rely on intensity information of images and requires a training phase for segmentation. Threshold and region based are conventional methods for brain tumor segmentation. In [5] local threshold value is determined based on

local statistics such as mean intensity value for segmenting different components of a image. In [6] Gaussian distribution is used to determine the threshold value. For region growing methods seeds can be selected manually or automatically. Region growing methods can effectively find the connected regions having similar properties. Watershed segmentation suffers over segmentation, so methods [7][8] were proposed to overcome this problem using prior knowledge from test images[9].

Automatic segmentation methods based on artificial intelligent techniques [10] do not rely on intensity information of images and requires a training phase for segmentation. Statistical pattern recognition [11] combines the information from a registered atlas template and user input. The method [12] requires prior definition of tumor boundaries. Expected maximization algorithm and atlas prior information is used in [13]. Tumors are considered as outliers and a statistical classification is used in [14]. But this method does not consider large deformation of brain structures. Brain tumor segmentation based on SVM [15] and alignment features [16] needs learning phase and user interaction. Prior cluster centre for specific tissue type learned from training data are used to construct multiple GMM based feature images[17]. In [18] this image segmentation algorithm are based on gray level values of pixels in edges Automatic seed selection for region growing[19] is done by selecting gray values sorted in frequency of occurrence which fails when different regions comprises of same intensity values.

III. PROPOSED METHOD

T1 C+ and FLAIR REL images are segmented for edema detection and to apply the feature extraction techniques. Fig.1 and Fig.2 illustrates the methodology of the proposed method for segmentation.

The main techniques for segmentation are histogram thresholding and region growing. Since the ring, centre and edema correspond to different intensity range in the two images, separate histograms are constructed for threshold computation. T1 C+ image is used for ring and centre of ring extraction. The ring centroid is used as a seed for region growing to segment the centre of the lesion.

In FLAIR image the lesion ring, centre appears less intense when compared with edema. Initially histogram thresholding is performed to extract the higher intensity region consisting of ring, centre and edema from the FLAIR image. The centre of this region is used as a seed point for region growing to segment the ring with its centre and subtracted from the output of histogram thresholding for edema detection as shown in Fig. 5. The main techniques used in this methodology are,

A. Threshold computation using Histogram
B. Region Growing algorithm

A. Threshold computation using Histogram

A histogram is plotted for the image with ‘n’ bins each of range‘t’(t=20). Since the ring area in ring enhancing lesions is hyperintense the threshold T is computed from higher intensity values of image as shown in Fig.3.The gray occurrence count n(r) is calculated where r is higher intensity range corresponding to the inhomogeneous hyper intense ring in the REL image. The count values are sorted

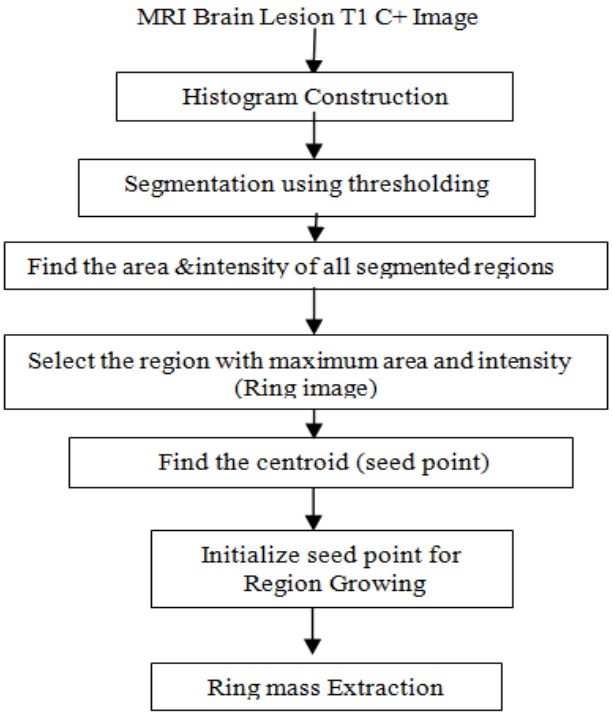

Fig. 1 Method for Ring and Ring mass extraction

in decreasing order. Let T be the intensity with highest count value. Thresholding is performed using Eq.1

$$f(x,y)=\begin{cases}0 \ if \ f(x,y) \neq T \\ 1 \ if \ f(x,y) = T\end{cases} \quad (1)$$

where $T=T-t \leq T \leq T+t$

B. Region Growing

Region based method is the most simple, robust, and effective method of segmentation. It is a procedure that starts in a seed point and group pixels into region based on some related feature[20].

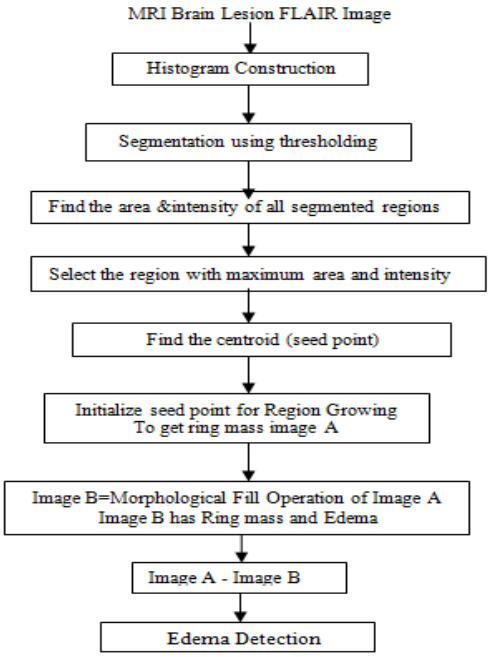

Fig. 2. Method for Edema Detection

Segmentation by region growing works by appending neighborhood pixels of seed point automatically selected from the region with maximum area in the resultant. The algorithm for implementing the seeded region growing algorithm is as follows:

Step 1: Assign the centre point of the region with maximum area from the image resulted from histogram thresholding as the seed point.

Step 2: Initialize the region mean equal to the pixel intensity at the seed point. Tolerance level is set as 20 from the mean intensity value.

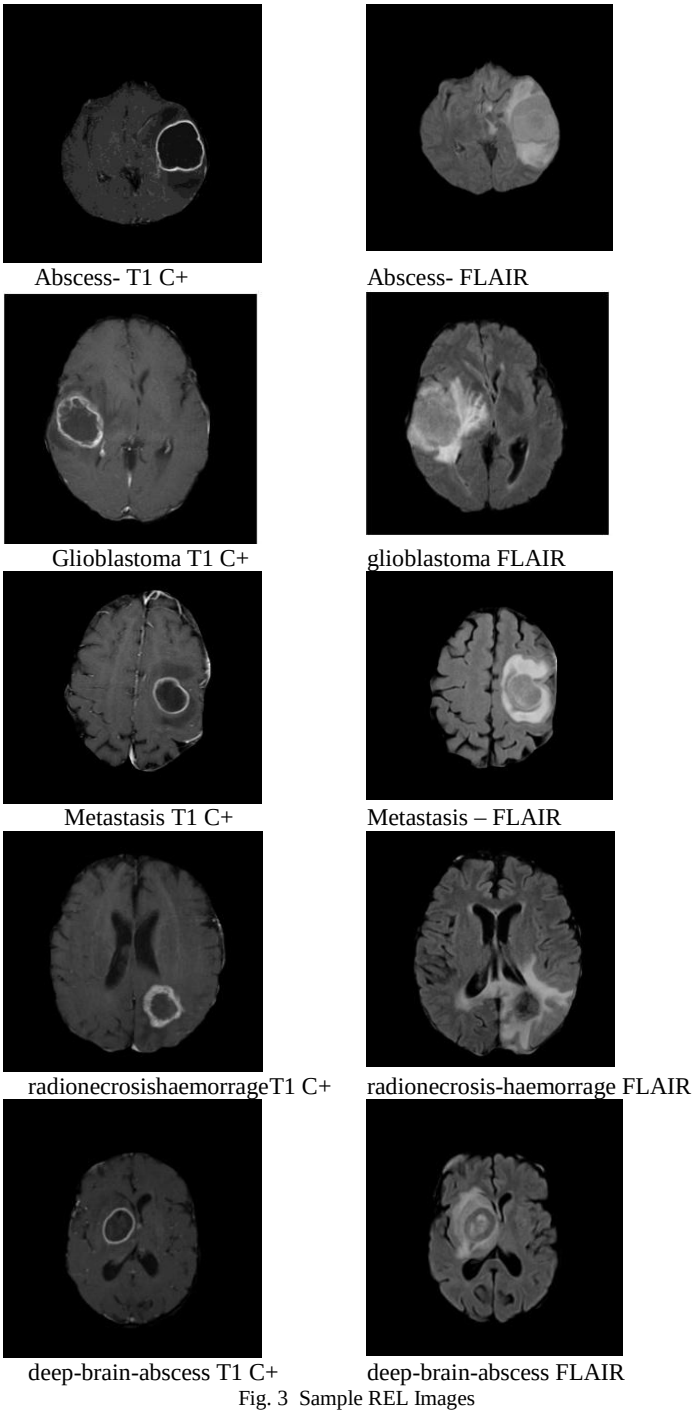

Fig. 3 Sample REL Images

Step 3: Compute the neighbours of the seed point and store them in the neighbour matrix, which stored the neighbouring pixels addresses, to be checked.

Step 4: For every pixel stored in the neighbor matrix, if the pixel is not labelled and the similarity criteria is fulfilled,

a) Label the pixel in the corresponding region.

b) Compute the new region mean of the corresponding region.

c) Compute the neighbours of the pixel and store them in the neighbour matrix if not labelled.

Step 5: Repeat the process until all pixels of the neighborhood matrix exceeds the tolerance level.

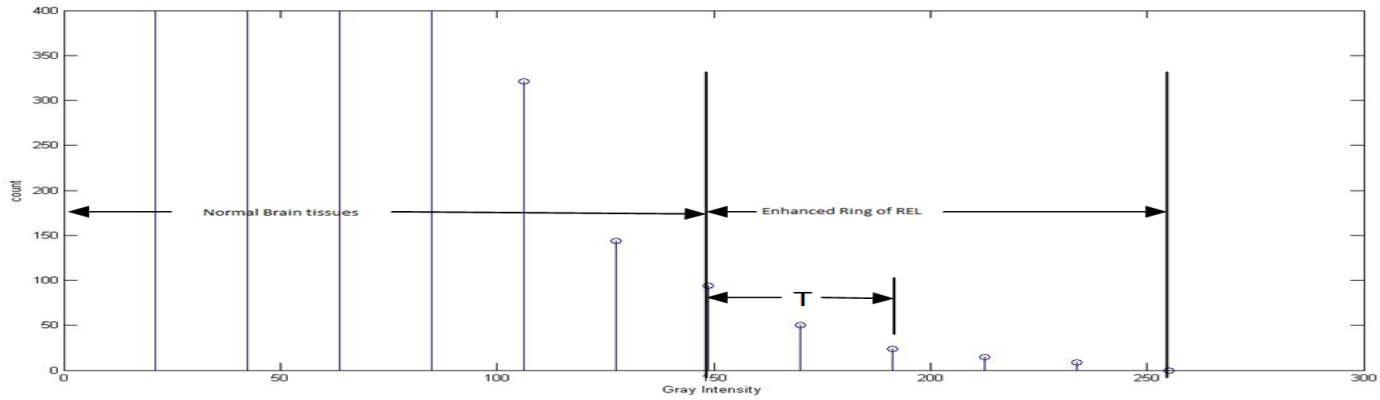

Fig.4. Computation of T for Metastasis T1 C+ using Histogram.

(a) (b) (c) (d)

Fig.5. Edema detection from glioblastoma FLAIR (a) Selected Region With Maximum Area(b) Morphological Fill Operation for Ring Centre+Edema Extraction (c) result of (Ring Centre+Edema) – Ring Centre (d) Edema Detection

TABLE I

VISUAL ANALYSIS OF REL SEGMENTATION

(GBM-GLIOBLASTOMA MULTIFORME, AB-ABCESS, MS-METASTASIS, RN-RADIONECROSIS, DBA-DEEP BRAIN ABCESS)

Images	Extracted Ring	Ring Centre	Edema Presence
AB			
GBM			
MS			
RN			
DBA			

IV FEATURE DESCRIPTORS FOR REL

Identifying different patterns on ring enhancement in the ring and its centre may help to differentiate [21] the REL. For e.g. Glioblastoma has thick& irregular ring, Abcess has thin & uniform ring with smooth inner and outer margin, Metastasis has uniform intense ring, and Radionecrosis single or multiple ring with unclear margin. The pattern of ring centre varies with necrosis, Haemorrhage or other fluids. Feature descriptors can be used to capture the pattern of lesions to aid diagnosis. Methods used for Texture, Statistical and shape descriptors are shown in fig. 6.

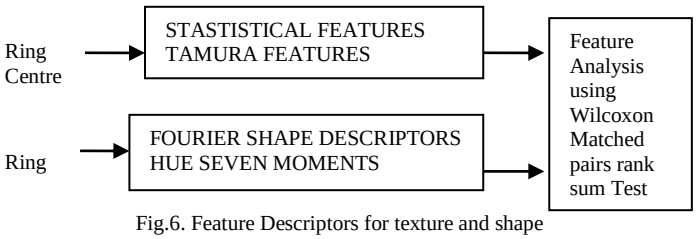

Fig.6. Feature Descriptors for texture and shape

A. Statistical Feature for Texture Description

Different tissues in REL centre possess different texture. Texture depend on the gray value

distribution and are calculated from image intensity values and its histogram. Texture vector T is computed using the formula shown in Table II [22] and the texture values are shown in Table III.

B. *Tamura Feature for Texture Description*

Based on human visual perception Tamura [23] propose six texture features: coarseness, contrast, directionality, line-likeness, regularity and roughness. The first three features are used to create three feature values in Table 1V.

Coarseness measures the size of texture elements and computed using the following steps,

1. For each pixel (x,y), find the average of 2^0X2^0 ,2^1X2^1 …2^5X2^5 windows.So k=0,1,2..5

2. Calculate the Absolute differences $E_k(x,y)$ for non overlapping averages in horizontal and vertical direction. In horizontal case it is given by Eq.2.,

$$E_{k,h}(x,y)=|A_k(x+2^{k-1},y)-A_k(x-2^{k-1},y)| \quad (2)$$

3. At each pixel find the value of k for which $E_{k,h}(x,y)$ is maximum. Set the best size $S_{best}=2^k$.

4. Coarseness is the average of S_{best} over the entire image.

Contrast defines the texture in terms of gray value range of pixels, polarization of black and white distribution, edge sharpness and periodicity of repeating patterns. It is defined by Eq.3

$$F_{contrast}=\sigma/(\alpha_4)^n \quad (3)$$

Where, $\alpha_4 = \mu_4/\sigma^4$, μ_4 is the fourth moment about the mean, σ is the variance. n=0.25 for closest agreements to human perception.

Directionality gives the texture orientation. For pixels greater than the threshold value, a quantized histogram $H_{dir}(a)$ is constructed with edge pixel count for corresponding directional angles . It is defined by Eq.4

$$F_{dir}=1\text{-}r\, n_{peaks}\sum_{p=1}^{n_{peaks}}\sum_{a\varepsilon w_p}(a-a_p)^2 H_{dir}(a) \quad (4)$$

Where,n_{peaks} is the no of peaks , a_p is position of p^{th} peak, w_p is the range of angles of p^{th} peak and r is the normalization factor.

C. *Moment Invariants for Shape Description*

Hu derived a set of moment invariants that can be used for shape analysis of objects irrespective of translation, scaling and orientation. The moments of MXM image with gray function f(x,y) translated by an amount(a,b) is given by Eq.5

$$\mu_{pq}=\sum_x\sum_y(x+a)^p\,.(y+b)^q\,f(x,y) \quad (5)$$

The scaling normalization of central moments is,

$\eta_{pq} = \mu_{pq} / \mu_{pq}^{\gamma}$, $\gamma= [(p+q)/2]+1$

The seven invariant moments are given by the following equation and their values are shown in Table V [24].

$M_1 = (\eta_{20} + \eta_{02})$

$M_2 = (\eta_{20} -\eta_{02})^2 + 4\eta_{11}^2$

$M_3 = (\eta_{30} - 3\eta_{12})^2 + (3\eta_{21}-\eta_{03})^2$

$M_4 = (\eta_{30} + \eta_{12})^2 + (\eta_{21}+\eta_{03})^2$

$M_5 = (\eta_{30} - 3\eta_{12})\ (\eta_{30} - \eta_{12})\ [(\eta_{30} - \eta_{12})^2 -3(\eta_{21}-\eta_{03})^2\ ] + (3\eta_{21}-\eta_{03})\ (\eta_{21}-\eta_{03})\ [\ 3(\eta_{30} - \eta_{12})^2- (\eta_{21}-\eta_{03})^2]$

$M_6 = (\eta_{20} -\eta_{02})\ [(\eta_{30} + \eta_{12})^2- (\eta_{21}+\eta_{03})^2\ ]\ 4\ \eta_{11}\ (\eta_{30} + \eta_{12})\ (\eta_{21}+\eta_{03})$

$M_7 = (3(\eta_{21}-\eta_{03})\ [(\eta_{30} + \eta_{12})[\ [(\eta_{30} + \eta_{12})^2- 3(\eta_{21}+\eta_{03})^2\ ]-(\eta_{30} +\eta_{12})\ (\eta_{21}+\eta_{03})[3(\eta_{30} + \eta_{12})^2- (\eta_{21}+\eta_{03})^2]$

D. *Fourier coefficients for Shape Description*

Fourier Descriptor [25] is the most robust contour based shape descriptor representing object in frequency domain. It applies Fourier transform on region boundary points and computes shape signatures in terms of Fourier coefficients. Large scale oscillations or general features are measured by first 50 coefficients and the later 50 coefficients measure smaller oscillations or finer details. The first 10 coefficients are used to construct the shape feature of ring image using the steps shown in fig.7. and the boundary approximation using the first ten coefficients is shown in fig.8.

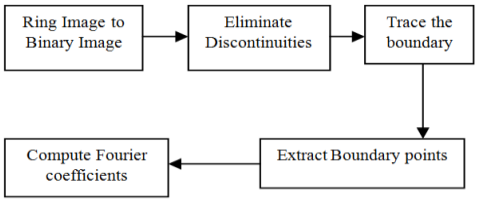

Fig .7. Shape Description using Fourier Descriptors

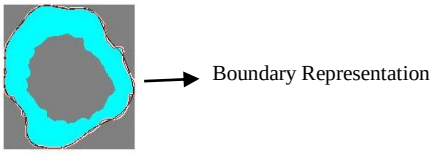

Fig. 8. Boundary of Radionecrosis ring using Fourier Coefficients

TABLE III
STATISTICAL FEATURES VALUES FOR TEXTURE

Texture	Moment	Expression	Description
T(1)	Mean	$M=\sum_{i=0}^{L-1} z_i P(z_i)$	Measure of average intensity
T(2)	Standard Deviation	$\sigma = \sqrt{\mu_2} = \sqrt{\sigma^2}$	Measure of average contrast
T(3)	Smoothness	$R=1-1/(1+\sigma^2)$	Relative intensity smoothness
T(4)	Histogram Skewness	$\mu_3= \sum_{i=0}^{L-1}(z_i-m)^3 p(z_i)$	Measure of Histogram symmetry
T(5)	Uniformity	$U=\sum_{i=0}^{L-1} p^2(z_i)$	Maximum when all intensity is equal
T(6)	Entropy	$e= -\sum_{i=0}^{L-1} p(z_i) log_2 p(z_i)$	Measure of Randomness

TABLE IIIII
STATISTICAL FEATURE VALUES FOR RING CENTRE

Images	T(1)	T(2)	T(3)	T(4)	T(5)	T(6)
GBM	29.079	43.67882	0.028504	3.461963	0.251639	3.673557
AB	21.66292	18.8933	0.00546	-0.01164	0.124755	4.234022
MS	23.26624	19.97608	0.006099	-0.00818	0.127959	4.382152
RN	21.66292	18.8933	0.00546	-0.01164	0.124755	4.234022
DBA	24.08154	18.44152	0.005203	-0.03064	0.094111	4.55619

TABLE IVV
TAMURA FEATURE VALUES FOR RING CENTRE

Images	Coarseness	Contrast	Directionality
GBM	35.6511	22.5564	1.0132
AB	40.1826	17.8906	0.97
MS	33.6018	18.266	1.0672
RN	31.2258	25.0188	1.1081
DBA	32.8008	16.8451	0.9791

TABLE V
HU'S SEVEN MOMENT INVARIANT VALUES FOR RING SHAPE

Image	M1	M2	M3	M4	M5	M6	M7
GBM	1.2347	0.1346	0.0499	0.0545	-0.0016	0.0116	0.0023
AB	1.9121	0.0482	0.1755	0.0067	0.0002	0.0014	0.0001
MS	1.6203	0.2803	0.0662	0.1234	-0.0071	-0.0441	0.0086
RN	0.8547	0.0526	0.0452	0.0104	0.0001	0.0022	-0.0002
DBA	4.4967	2.8853	12.1624	14.1376	185.3654	22.6936	2.6538

TABLE VI
FOURIER COEFFICIENT VALUES FOR RING BOUNDARY DESCRIPTION

Images	Coeff1	Coeff2	Coeff3	Coeff4	Coeff5	Coeff6	Coeff7	Coeff8	Coeff9	Coeff10
GBM	2.8284	3.7993	8.3975	3.8741	2.6295	6.4459	3.0901	5.090	8.109	1.223
AB	4.2426	9.64	2.4867	5.9909	4.5883	3.1098	4.2655	9.4474	3.6791	5.6037
MS	4.1231	4.725	3.6153	2.0013	3.5878	3.3433	5.8881	2.2223	6.7736	0.4817
RN	3.6056	6.9882	9.7789	2.7071	4.5156	7.1874	7.0445	8.72	5.5195	0.5922
DBA	6.4031	7.599	1.9865	6.2399	3.0429	6.2463	1.4615	3.095	2.1894	7.7329

V. EXPERIMENTAL ANALYSIS AND DISCUSSION

The algorithm is implemented in Matlab R2010a. Fig.4. shows T1 C+ and Flair axial MRI images used for segmentation. For quantitative analysis, Success rates and similarity metrics are

computed. Four parameter true positive (TP), false positive (FP), true negative (TN), false negative (FN) are calculated by the logical AND between ground truth and segmented image. Success rates are usually defined by sensitivity and specificity.

Sensitivity is also named as target overlap that is the intersection between two similarly labeled regions r in G and A over the extent of G volume given by Eq.7

$$\text{Sensitivity}=\frac{TP}{TP+FN} \quad (7)$$

Specificity is defined as the fraction of the non-target-object voxels over the non-ground-truth voxels (Equation). That is, the fraction of the negative samples which are also labeled as negative by the to-be-evaluated segmentation method given by the following equation Eq.8 [26],

$$\text{Specificity}=\frac{TN}{TN+FP} \quad (8)$$

The similarity metrics Dice and Jaccard coefficient [27] quantify the spatial overlap between ground truth and segmented image. Jaccard coefficient or union overlap that is defined as the intersection between two similarly labelled regions r over their union given by the following equation Eq.9

$$\text{Jaccard}=\frac{|TP|}{|TP|+|FP|+|FN|} \quad (9)$$

Dice coefficient [28] or mean overlap as a special case of the Kappa coefficient. Dice is defined as the intersection between two similarity labeled regions r in G and A over the average volume of these two regions given by equation Eq.10 .

$$\text{Dice}=2\frac{|TP|}{(|TP|+|FP|+|TP|+|FN|)} \quad (10)$$

The quantitative results are shown in table 2. The results prove the performance of the proposed method. The visual analysis from Table I shows that, region growing is efficient in clustering related pixels and the tumor edges are extracted efficiently. As the image is threshold initially and the region is extracted, the computation is reduced. The computation is reduced as the region growing is adopted only on the region cropped based on thresholding. This method is very efficient to calculate the local features of ring enhancing lesion which can be used for image retrieval as it is automatic, simple and requires less computation.

TABLE VVI
QUANTITATIVE RESULTS FOR RING SEGMENTATION FOR DIFFERENT REL IMAGES

Images	Sensitivity (%)	Specificity (%)	Accuracy (%)	Jaccard Index (%)	Dice Coefficient (%)
AB	96.5	97.7	97.35	92.0	95.8
GBM	96.9	97.3	97.0	93.7	96.7
MS	98.9	97.5	98.0	95.2	97.5
RN	99.1	96.4	97.8	96.6	98.0
DBA	99.4	99.5	99.7	99.6	99.0

VI. FEATURE ANALYSIS

Wilcoxon Matched pairs rank sum Test is used to calculate the difference between the sum of ranks of two independent samples. The features are significantly different if $p<0.5$ otherwise $p>0.5$[29].Feature analysis using the texture and shape descriptors are shown in the table VIII TO table XI . From the tables, the feature vector x and y of two different images are symmetric in nature.
i.e $F(x,y)=F(y,x)$. Table VIII shows statistical feature descriptor can differentiate texture by 40% . Ring in GBM and DBA are more similar which can be differentiated by the intensity of ring mass in T1 and T2 images. Since the texture in ring mass is homogenous and less coarse, tamura feature is not effective for feature extraction in REL. Table XI shows Fourier descriptors are good to discriminate shape as 80% values are $p<0.6$.

TABLE VIII
FEATURE ANALYSIS USING STATISTICAL DESCRIPTOR FOR TEXTURE

Image	GBM	AB	MS	RN	DBA
GBM	1	0.4848	0.4848	0.4848	0.4848
AB	0.4848	1	0.6991	1	0.9372
MS	0.4848	0.6991	1	0.6991	0.9372
RN	0.4848	1	0.6991	1	0.9372
DBA	0.4848	0.9372	0.9372	0.9372	1

TABLE VIX
FEATURE ANALYSIS USING TAMURA DESCRIPTOR FOR TEXTURE

Image	GBM	AB	MS	RN	DBA
GBM	1	1	1	1	0.700
AB	1	1	1	1	1
MS	1	1	1	1	0.700
RN	1	1	1	1	1
DBA	0.700	1	1	1	1

TABLE X
FEATURE ANALYSIS USING MOMENT INVARIANTS FOR SHAPE

Image	GBM	AB	MS	RN	DBA
GBM	1	0.7104	1	0.4557	5.8275e-004
AB	0.7104	1	0.9105	0.8333	5.8275e-004
MS	1	0.9105	1	0.7104	5.8275e-04
RN	0.4557	0.8333	0.7104	1	5.8275e-04
DBA	5.8275e-004	5.8275e-004	5.8275e-04	5.8275e-04	1

TABLE XI
FEATURE ANALYSIS USING FOURIER COEFFICIENTS FOR SHAPE

Image	GBM	AB	MS	RN	DBA
GBM	1	0.427	0.5205	0.3447	0.8501
AB	0.427	1	0.1405	0.6776	0.5708
MS	0.5205	0.5205	1	0.0757	0.6232
RN	0.3447	0.6776	0.0757	1	0.3847
DBA	0.8501	0.5708	0.6232	0.3847	1

VII. CONCLUSION LIMITATIONS AND FUTURE WORK

Thresholding makes the Segmentation fast and Region growing improves the accuracy of result. The method is fully automatic and based on the diagnostic properties of image. Fourier coefficients accurately estimates the shape of the ring.In this method T1and FLAIR images are considered. Certain tumors appear bright in T1 but dark in T2, so including all the image modalities can improves the accuracy of diagnosis. An automatic Brain skull removal method should be added with this technique. The ring and centre of ring are segmented but only the presence of edema is detected. Though edema presence is enough for initiating anti edema treatment and differentiating REL, The future work will be accurate segmentation of edema and predicting the lesion. Also this method can be used for local feature extraction for tumor retrieval systems. The sample images are from [21], in future real time images would be tested for REL segmentation and feature extraction to develop a retrieval system.

REFERENCES

[1] Geoff Dougherty, "Digital Image Processing for Medical Applications", Cambridge University Press,2009

[2] Clark, M.C., Hall, L.O., Goldgof, D.B., Velthuizen, R., Murtagh, F.R., Silbiger, M.S., 1998. Automatic tumor-segmentation using knowledge-based techniques. IEEE Transactions on Medical Imaging 117, 187–201.

[3] N. Sharma and L. M. Aggarwal,Automated medical image segmentation techniques, Journal of Medical Physics/Association of Medical Physicists of India, vol. 35,
no. 1, p. 3, 2010.

[4] S. Bauer, R. Wiest, L.-P. Nolte, and M. Reyes, A survey of mri-based medical image analysis for brain tumor studies,Physics in Medicine and Biology, vol. 58, no. 13, p. R97,2013.

[5] Y.-C. Sung, K.-S. Han, C.-J. Song, S.-M. Noh, and J.-W.Park, Threshold estimation for region segmentation on mr image of brain having the partial volume artifact, in SignalProcessing Proceedings, 2000. WCCC-ICSP 2000. 5th International Conference on, IEEE, 2000, vol. 2, pp. 1000-1009.

[6] A. Stadlbauer, E. Moser, S. Gruber, R. Buslei, C. Nimsky,R. Fahlbusch, and O. Ganslandt, Improved delineation of brain tumors: An automated method for segmentation based on pathologic changes of 1H-MRSI metabolites in gliomas, Neuroimage, vol. 23, no. 2, pp. 454-461, 2004

[7] A. Bleau and L. J. Leon, Watershed-based segmentation and region merging, Computer Vision and Image Understanding, vol. 77, no. 3, pp. 317-370, 2000.

[8] V. Gies and T. M. Bernard, Statistical solution to watershed over-segmentation, in International Conference on Image
Processing, 2004

[9] S. D. Salman and A. A. Bahrani, Segmentation of tumor tissue in gray medical images using watershed transformation methods, International Journal of Advancements in Computing Technology, vol. 2, no. 4, pp. 123-127, 2010.

[10] Clark, M.C., Hall, L.O., Goldgof, D.B., Velthuizen, R., Murtagh, F.R., Silbiger, M.S., 1998. Automatic tumor-segmentation using knowledge-based

techniques. IEEE Transactions on Medical Imaging 117, 187–201.

[11] Kaus, M.R., Warfield, S.K., Nabavi, A., Chatzidakis, E., Black, P.M.,Jolesz, F.A., Kikinis, R., 1999. Segmentation of meningiomas and low grade gliomas in MRI. In: Taylor,C., Colchester, A.(Eds.), Lecture Notes in Computer Science, MICCAI, vol. 1679. Springer,pp1–10.

[12] Cuadra, M.B., Gomez, J., Hagmann, P., Pollo, C., Villemure, G., Dawant, B.M., Thiran, J.-Ph., 2002. Atlas-based segmentation of pathological brains using a model of tumor growth. In:Medical Image Computing and Computer-Assisted Intervention MICCAI 2002, Springer, pp.380–387.

[13] N. Moon, E. Bullitt, K.V. Leemput, and G. Gerig. Model-based brain and tumor segmentation. In ICPR, pages 528–531, Quebec, August 2002.

[14] M. Prastawa, E. Bullitt, S. Ho, and G. Gerig. A brain tumor segmentation framework based on outlier detection. Medical Image Analysis, 18(3):217–231, 2004

[15] M. Schmidt, I. Levner, R. Greiner, A. Murtha, and A. Bistritz. Segmenting Brain Tumors using Alignment-Based Features. In IEEE International Conference on Machine learning and Applications, pages 215–220, 2005.

[16] J. Zhou, K.L. Chan, V.F.H Chong, and S.M. Krishnan. Extraction of brain tumor from MR images using one-class support vector machine. In IEEE Conference on Engineering in Medicine and Biology, pages 6411– 6414, 2005.

[17] B. B. Avants, N. J. Tustison, J. Wu, P. A. Cook, and J. C. Gee, "An open source multivariate framework for n-tissue segmentation with evaluation on public data," Neuroinformatics, vol. 9, no. 4, pp. 381–400, Dec. 2011.

[18] G. M. N. R. Gajanayake, R. D. Yapa1 and B. Hewawithana, "Comparison of Standard Image Segmentation Methods for Segmentation of Brain Tumors from 2D MR Images", 4th International Conference on Industrial and Information Systems, ICIIS, University of Peradeniya, Sri Lanka, pp. 301-305., IEEE, 2009.

[19] Shweta Kansal, Pradeep Jain , Automatic Seed Selection Algorithm For Image Segmentation Using Region Growing,International Journal of Advances in Engineering & Technology, June, 2015. Vol. 8, Issue 3, pp. 362-367

[21] http://eradiology.bidmc.harvard.edu/LearningLab/central/OConnell.pdf

[22] Gonzalez, R.C. Richard, E.W, "Digital Image Processing,"(2004), II Indian Edition, Pearson Education, New Delhi, India.

[23] H.Tamura ,S.Mori ,and T.Yamawki, "Textural features corresponding to visual perception ",IEEE Transactions on Circuits and Systems for video Technology, vol. 11,8,no.6,pp 460-473,1978

[24] Hu M 1962 Visual pattern recognition by moment invariants. *IRE Trans. Inf. Theor.* IT-8: 179–187

[25] D.Zang G Lu , " Review of Shape Representation and description techniques",Pattern Recognition, vol 37 (1),pp 1-19,2004

[26] Shattuck, d.w., prasad, g., mirza, m., narr, k.l. and toga, A.W., 2009 April. Online resource for validation of brain segmentation methods. NeuroImage, 45(2), pp. 431-439.

[27] Jaccard, P., 1912 Febrruary, The Distribution of the Flora in the Apline Zone,New Phytologist, 11(2), pp. 37-50.

[28] Dice, L.R., 1945July,Measures of the amount of ecologic association between species,Ecology,pp.297-302.

[29] C.P. Loizou, C.S. Pattichis, I. Seimenis, M. Pantziaris, ,"Quantitative Analysis of Brain White Matter Lesions in Multiple Sclerosis Subjects" Proceedings of the 9th International Conference on Information Technology and Applications in Biomedicine, ITAB 2009, Larnaca, Cyprus, 5-7 November 2009

[21] https://radiopaedia.org